

Surface conductivity of the honeycomb spin-orbit Mott insulator Na₂IrO₃

Thomas Dziuba, Ina-Marie Pietsch, Máté Stark, Georg A. Traeger, Philipp Gegenwart, Martin Wenderoth

Angaben zur Veröffentlichung / Publication details:

Dziuba, Thomas, Ina-Marie Pietsch, Máté Stark, Georg A. Traeger, Philipp Gegenwart, and Martin Wenderoth. 2021. "Surface conductivity of the honeycomb spin-orbit Mott insulator Na₂IrO₃." *physica status solidi (b)* 258 (1): 2000421.
<https://doi.org/10.1002/pssb.202000421>.

Surface Conductivity of the Honeycomb Spin–Orbit Mott Insulator Na_2IrO_3

Thomas Dziuba,* Ina-Marie Pietsch, Máté Stark, Georg A. Traeger, Philipp Gegenwart, and Martin Wenderoth

The search for materials with novel and unusual electronic properties is at the heart of condensed matter physics as well as the basis to develop conceptual new technologies. In this context, the correlated honeycomb transition metal oxides have attracted large attention for both, being a possible experimental realization of the theoretically predicted magnetic Kitaev exchange and the theoretical prospect of topological nontriviality. Mott-insulating Na_2IrO_3 is prototypical among these materials, characterized by crystal field splitting, spin–orbit coupling, and Hubbard repulsion being on similar energy scales. Herein, a combined electrical transport and scanning tunneling spectroscopy (STS) study of the surface of sodium iridate cleaved and in situ investigated under ultrahigh vacuum is reported. Temperature-dependent transport measurements prove the existence of surface conductance with a surprisingly high and temperature-independent conductivity. STS shows a variety of different spectra. Most importantly, a significant density of states is found within the bandgap of sodium iridate at the surface. Based on the local spectroscopic information, multiple conductive channels with differing nature being simultaneously apparent in this material are discussed.

focuses on sodium iridate (Na_2IrO_3), that consists of alternately stacked Na_3 and NaIr_2O_6 layers (see Figure S1, Supporting Information), where the structure of the NaIr_2O_6 layer with a honeycomb coordination is determined by iridium atoms surrounded by edge-sharing oxygen octahedra providing the basic ingredients for the magnetic Kitaev exchange interaction.^[1–6] The electronic properties are highly complex, as crystal field splitting, strong spin–orbit coupling, and Hubbard repulsion have similar energy scales in Na_2IrO_3 .^[1,6–14] Na_2IrO_3 was shown to be a robust $J_{\text{eff}} = 1/2$ Mott insulator with a bandgap comparable with common semiconductors.^[8,15,16] Although the magnetic properties of Na_2IrO_3 are dominated by the strongly bond-dependent Kitaev exchange, the admixture of Heisenberg, and off-diagonal interactions beyond nearest neighbors leads to a zigzag antiferromagnetic-ordered ground state.^[2,17–19]

Furthermore, Na_2IrO_3 is theoretically considered as a candidate material for correlated topological insulator behavior.^[9–11,20,21]


1. Introduction

Correlated honeycomb transition metal oxides (TMOs) A_2IrO_3 ($\text{A} = \text{Li}, \text{Na}$) attract large attention for being at the intersection of various physical phenomena that are in the focus of current research due to their potential relevance for future technological application as well as for fundamental questions. This work

To this end, many groups have investigated the surface properties of Na_2IrO_3 , but no consistent picture has been obtained from the experimentally determined electronic and transport data. Optical conductivity, angle-resolved photoemission spectroscopy (ARPES), and scanning tunneling spectroscopy (STS) investigations reported a wide range of bandgaps between 340 meV and 1.2 eV.^[8,15,16] Scanning tunneling microscopy (STM) and scanning tunneling spectroscopy (STS) experiments on freshly cleaved Na_2IrO_3 crystals found a bandgap of 1.2 and 0.6 eV, associated with a $\text{Na}_3[(1 \times 1)]$ - and $\text{NaIr}_2\text{O}_6[(\sqrt{3} \times \sqrt{3})\text{R}30^\circ]$ -surface reconstruction, respectively.^[15] Spatially resolved ARPES investigations also found different bandgap widths for the two surface terminations.^[16] However, the extracted absolute values are not consistent with the STS investigations. Only recently, first indications of density of states at or close to the Fermi level have been reported from ARPES measurements.^[22,23] Transport investigations have reported a freeze-out of conductivity at low temperature.^[16,23,24] Investigations using conductive AFM under ambient condition showed the formation of sodium clusters at the surface of Na_2IrO_3 when exposed to air for several hours, resulting in metallic-like conductivity on the surface, which was attributed to the sodium

T. Dziuba, M. Stark, G. A. Traeger, Dr. M. Wenderoth
Physical Institute
Georg-August University Göttingen
Friedrich-Hund-Platz 1, 37077 Göttingen, Germany
E-mail: thomas.dziuba@uni-goettingen.de

I.-M. Pietsch, Prof. P. Gegenwart
Experimental Physics VI
Center for Electronic Correlations and Magnetism
Augsburg University
Universitätsstraße 1, 86159 Augsburg, Germany

 The ORCID identification number(s) for the author(s) of this article can be found under <https://doi.org/10.1002/pssb.202000421>.

© 2020 The Authors. Published by Wiley-VCH GmbH. This is an open access article under the terms of the Creative Commons Attribution License, which permits use, distribution and reproduction in any medium, provided the original work is properly cited.

DOI: 10.1002/pssb.202000421

clusters.^[25] In summary, in addition to the in-gap states observed by ARPES, neither a clear bandgap closing by surface states in spectroscopic data nor surface conductivity has been reported.^[16,22,23]

In this work, we combine temperature-dependent transport measurements with STM and STS investigations on freshly cleaved Na₂IrO₃ single crystals under ultrahigh vacuum (UHV) conditions. We have found a surprisingly high conductivity on the Na₂IrO₃ surface in transport measurements as well as an in-gap local density of states at the surface in local spectroscopy. Our approach gives access the local surface structure (e.g., defects) as well as possible degradation which is included in the interpretation. The combination of local spectroscopy and transport data allows disentangling different conductivity channels. We propose a model which classifies the conductive behavior inside the bulk bandgap as well as the conductive behavior of the Na₂IrO₃ surface.

2. Sample Synthesis and Investigation Methods

The samples were grown using solid-state synthesis, resulting in thin plate-shaped crystals with a diameter of up to 4 mm. The preceding polycrystalline material was grown and characterized, as described in former works.^[14,24] After adding 10% extra Ir powder, the mixture was heated up to 900 °C, cooled and ground. Afterward, the product was heated to 1050 °C. This results in small single crystals. Larger crystals were obtained by an additional annealing with slow heating to 1050 °C followed by a long hold time. Magnetic susceptibility measurements carried out with a Quantum Design MPMS3 revealed a sharp signature

at T_N , confirming good crystalline quality (for details, see Figure S2, Supporting Information).

For bulk and surface conductivity measurements, four gold contacts were attached to the Na₂IrO₃ crystals, using evaporation of high-purity gold and shadow masks (Figure 1a–c). Two contacts, A and B, are located on the top side of the sample, whereas contacts C and D are contacting the rear side. The contacts of each pair (top/bottom) were positioned at laterally opposite sides of the crystal. To achieve a clean surface, crystals were cleaved, and in situ investigated under UHV conditions. Temperature-dependent I – V measurements were done using a Keithly 2602B source measure unit. Cooling was done using a LN₂-cryostat that is thermally connected to the sample stage. Temperature measurements were carried out using a k-type thermocouple attached to the stage. After carrying out all measurements, an additional k-type thermocouple was attached directly to the sample surface to check for the discrepancy of measured temperature at the stage and on the sample surface. The accordingly corrected temperature scale is used in all displayed data.

Atomic-scale characterization was done in a bespoke UHV STM at pressures below 5×10^{-10} mbar at 300 and 80 K on multiple crystals. STM topography images were acquired using constant current mode. All voltages refer to the sample bias voltage with respect to the tip, all currents refer to the tunneling current between tip and sample. To gain STS maps dI/dV spectra were recorded at every second pixel in the topography using lock-in techniques. In parallel, I – V curves were recorded without lock-in techniques and used for the calibration of the dI/dV curves. The absolute calibration error can be estimated to $<0.5 \text{ pA V}^{-1}$ at free surfaces and $<2.6 \text{ pA V}^{-1}$ at step edges due to a lower signal to noise ratio. Tungsten STM tips were

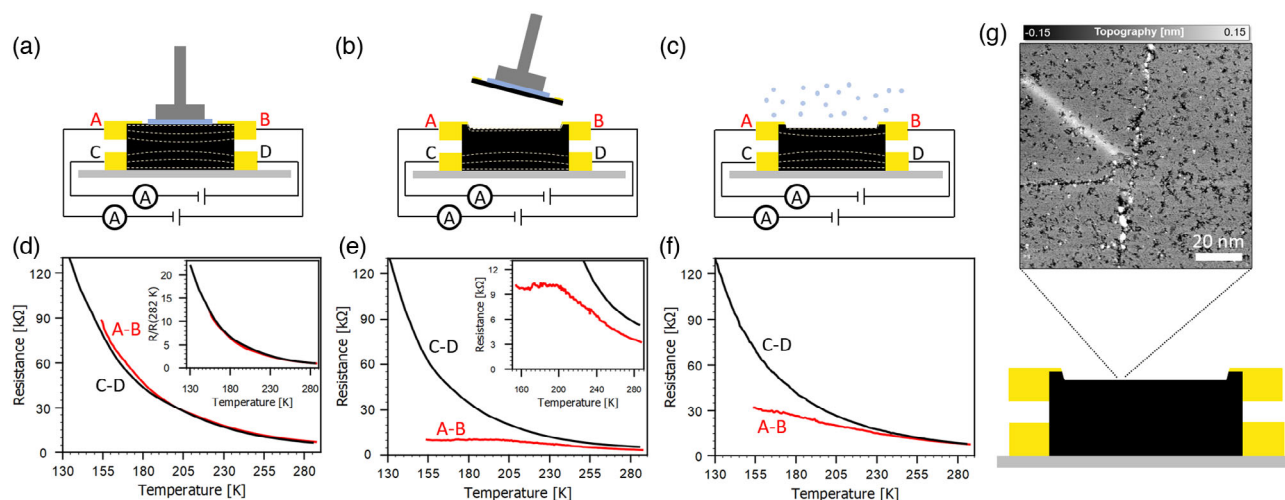


Figure 1. Surface conductivity of cleaved Na₂IrO₃. To distinguish surface-related conductivity from bulk conductivity, four contacts were attached to the sample: two for contacting the (freshly cleaved) crystal surface (A–B) and two for reference measurements through the uncleaved crystal (C–D). a) Before cleavage, measurements of the bulk conductivity were done for both channels. The yellow dashed lines mark the anticipated current flow. d) The conductivity of the bulk crystal shows a strong temperature dependence between 285 and 154 K. The experimental results can be modeled with thermal activation at higher temperatures, resulting in excitation energies of 195 and 205 meV for the channels A–B and C–D, respectively. b) After cleaving in UHV, e) the conductivity at low temperatures is completely dominated by the surface, reducing the resistivity by nearly an order of magnitude at 155 K. c) After exposing the surface by air for several hours, f) the surface conductivity is reduced but not completely suppressed. g) $100 \times 100 \text{ nm}^2$ constant current topography of the freshly cleaved surface. Defects ranging from vacancies to cracks and ridge-like defects are always apparent, making the high conductivity (see (d)) even more remarkable. For further topographic details see Figure S3, Supporting Information.

prepared by electrochemical etching in a KOH solution and further processed by annealing and argon sputtering in UHV. During measurement, modifications of the tip by Na desorption or adsorption occur by chance due to the high sodium mobility on the Na_2IrO_3 surface. Intentional cleaning of the tip is done by applying voltage pulses up to 5 V.

3. High Surface Conductivity of Na_2IrO_3 in Transport Measurements

The high reactivity of Na_2IrO_3 leads to the rapid degradation of its surface under ambient conditions.^[26] To avoid this problem, the temperature-dependent transport measurements are carried out in an UHV setup on in situ-cleaved single crystals. Bulk properties of our sample have been acquired using both channels (A–B, C–D) before cleavage (Figure 1d), showing the well-known freeze out of conductivity at lower temperature.^[16,24] Modeling these curves with a simple thermal excitation Ansatz $R \approx \exp(\Delta E/2k_B T)$ for high temperatures (>240 K) yields excitation energies of $\Delta E_{AB} = 195$ meV and $\Delta E_{CD} = 205$ meV for the channels, A–B and C–D, respectively. It is worth noting that these values are a lower boundary as the previously reported hopping mechanism contributes to the overall conductivity of the material, which is not reflected by the thermal activation calculation.^[24]

After cleaving, we observe a significant increase in the conductivity along the surface (channel A–B, Figure 1e). In contrast, the conductivity of the bulk remains unaffected (channel C–D, Figure 1e). While the bulk conductivity can be modeled based on thermal excitation and variable range hopping, the surface conductivity is characterized by a temperature-independent resistivity below ≈ 200 K without any indication of a freezing out of conductivity. The average resistance of around $10 \text{ k}\Omega$ below 200 K corresponds to a 2D sheet resistance between 0.5 and $2 \text{ k}\Omega \square^{-1}$, depending on the estimated contact area between the gold contacts and the sample surface that was evaluated using an optical microscope. For temperatures >200 K, the shape of the $R(T)$ curve still resembles the qualitative behavior of the bulk conduction being explained by thermal excitation and variable range hopping but with a reduced overall resistivity. To further investigate the surface conductivity, we expose the surface for 13 h to air, resulting in an overall reduction of the surface conductivity Figure 1f. Considering the reported high reactivity of the surface in ambient air, the degradation of the surface conductivity is surprisingly slow.^[26]

In contrast to previous transport measurements, which have only reported a strong temperature-dependent thermally activated and hopping-mediated conductivity, our data show the clear signature of a low resistivity surface-related conducting channel for a freshly cleaved sample.^[16,23,24] We find a change of sign of the derivative of the conductivity $d\rho/dT$ at ≈ 200 K, separating the high conductivity regime at lower temperatures from the Mott-insulation regime above 200 K. Our results showing a temperature-independent high conductivity surface channel imply that previous transport investigations, being conducted on uncleaved crystals, are dominated by bulk conductivity.^[16,23,24]

4. Spectroscopic Characterization of Na_2IrO_3 Surface States

The high surface conductivity implies a density of states close to the Fermi level. To further analyze this issue, we complement our transport measurements with a STM and STS study on surfaces investigated under identical conditions, i.e., on surfaces freshly cleaved in UHV.

In constant current topography measurements, we observe the known (1×1) as well as the $(\sqrt{3} \times \sqrt{3})\text{R}30^\circ$ reconstructions.^[15,16] In agreement with previous STM investigations, only the sodium terminated (1×1) surface appears to be well ordered for large areas, where the $(\sqrt{3} \times \sqrt{3})\text{R}30^\circ$ reconstruction exhibits particularly high defect densities and merely small well-ordered patches.^[15] To investigate the properties of the surface, we focus on the (1×1) sodium termination. For the sake of completeness, according data for the $(\sqrt{3} \times \sqrt{3})\text{R}30^\circ$ reconstruction is found in Figure S4, Supporting Information.

Based on our collective STM/STS data, we identify three generic classes of spectra. Prototypical room-temperature datasets of these spectra are shown in Figure 2. It is worthwhile to mention that the discussed data are all observed on clean surfaces, i.e., visible defects in the surface which are always present are at least a few atoms apart.

Type 1 spectra show a clear bandgap of 0.8 eV at room temperature close to previous STM results.^[15] We refer to this gap between valence band edge at -0.45 eV and the conduction band edge at 0.35 eV in the following as the “bulk bandgap,” being aware that this value was found to be different on the two surface reconstructions.^[15] Most importantly, these type of spectra shows no hallmark of in-gap local density of states.

Type 2 spectra exhibit additional peaks at -0.5 and 0.5 eV labeled as D and D* close to the valence and conduction bands. These peaks are “symmetrically” broadened over several hundred millielectronvolts each. The in-gap conductivity has a minimum at the Fermi level.

Type 3 spectra paint a very different picture: the bandgap is entirely closed in a V-shaped fashion, with the minimum at the Fermi level. The onset of tunneling into the valence and conduction band states is visible at -0.5 and 0.5 eV as a change of the slope, indicated by arrows.

As the transport measurements were carried out from low temperature to room temperature, we have also taken STM and STS data at 80 K, as shown in Figure S5, Supporting Information. In general, we find all three spectral types. Based on our current statistics, type 2 spectra are severely underrepresented at 80 K, i.e., for a given number of surface examinations on different positions, the spectra of type 2 occur significantly less frequent at 80 K compared with 300 K.

Considering the large amount of data for multiple STM tips, samples, lateral positions on the respective sample surface as well as measurements at different temperatures, we interpret the spectral types 1, 2, and 3 as intrinsic sample properties. We discovered that the addressability of the different states underlying the spectroscopic data is also dependent on extrinsic properties, e.g., surface defects like vacancies and surface steps as well as the tip properties. Further data are found in Figure S6, Supporting Information, displaying the simultaneous

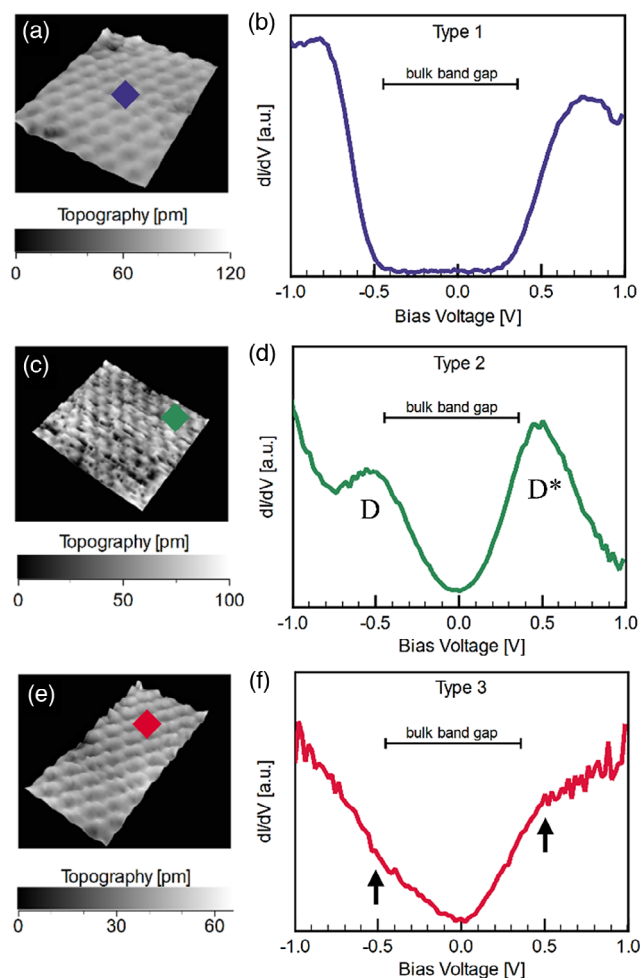


Figure 2. Three observable generic types of spectra and the corresponding topographies of the (1×1) -reconstructed surface. All acquired spectra can be sorted according to simple criteria. a,b) Type 1: a bandgap of 0.8 eV at room temperature is very pronounced with no residual in-gap conductivity. c,d) Type 2: In-gap differential conductivity showing broad, Gauss-shaped peaks at -0.5 and 0.5 V bias voltage and labeled by D and D^* . e,f) Type 3: these dI/dV spectra are characterized by a V-shaped bandgap closing and a minimum of conductance close to the Fermi level. The onset of tunneling out of the valence and into the conduction bulk band is visible as small shoulders, indicated by arrows.

occurrence of all three spectral types in a single dataset, also showing the impact of the tip on the spectra. A full discourse on this can be found in the Supporting Information. Finally, we like to mention that the highly reactive surface prohibited a controlled tip preparation (further discussion on this is found in the Supporting Information).

5. Discussion

Our transport measurements reveal the existence of two different conducting channels. First, the known (bulk)conductivity from thermally activated charge carriers (dominating at high temperatures 200–300 K) and variable range hopping (taking over at

lower temperatures).^[24] And second, the newly discovered surface conductivity which does not freeze out with decreasing temperature. In the following, we develop a comprehensive model which link the different spectral types to the transport results on freshly cleaved Na_2IrO_3 crystals.

We propose that type 1 spectra corresponds to the gap between the lower and the upper Hubbard bands, i.e., denoting the previously called “bulk bandgap” to be the underlying Mott gap. Moreover, due to the large value of the gap, type 1 spectra do not have a counterpart in transport.

We start the interpretation of the transport and STS findings for the bulk conductivity. The thermal excitation Ansatz yields an activation energy of ≈ 0.2 eV derived from the transport data. Our STS data (types 1, 2, and 3) suggest that the Fermi energy is—at least at the surface—located close to the center of the bandgap. As the (bulk-)bandgap as taken from type 1 spectra is much larger (0.8 eV at 300 K, see Figure 2b), we propose that the activation energy determined from macroscopic experimental data can be attributed to excitations either within D or D^* states or between the two.^[8,16,22] Within this model, type 2 conductivity masks the underlying energy gap shown by type 1 spectra.

The question of the physical origin of type 2 spectra remains and is discussed in the following paragraphs.

It was recently reported for Na_2IrO_3 and other $J_{\text{eff}} = 1/2$ systems like $\text{Sr}_3(\text{Ir}_{1-x}\text{Ru}_x)_2\text{O}_7$ and $(\text{Sr}_{1-x}\text{La}_x)_2\text{IrO}_4$ that both, disorder and doping can result in the narrowing or even closing of the Mott gap.^[16,27,28] It was shown that this gap closing gradually correlates with the degree of doping or defect density, where it is the actual valence and conduction band edges that move closer to the Fermi level. On the one hand, we observe a high defect density potentially inducing local disorder, and on the other hand, a termination-dependent quasiparticle charge transfer was shown by spatially resolved ARPES to exist for sodium iridate, resulting in effective doping.^[16] Both, prior STM and spatially resolved ARPES investigations found two different reconstructions and have determined a corresponding Mott gap. But while STM reported the larger bandgap for the (1×1) surface, where the surface has a sodium deficit of $1/6$ compared with the bulk, spatially resolved ARPES reported the larger bandgap for the $(\sqrt{3} \times \sqrt{3})\text{R}30^\circ$ reconstruction, where according to the model developed by Lüpke et al., the surface misses $4/6$ of the sodium relative to the bulk.^[15] Even though a doping effect cannot be entirely neglected as the cause for the observation of two different energy gaps (type 1 and type 2), this would either imply concurrent spectral observations for the very same (Hubbard-)bands or that the STM and ARPES investigations generally observed somehow different surfaces.^[15,16] Consequently, this renders this explanation to be questionable, and we propose a simpler model that is equally fit to explain the findings.

As our main analysis is restricted to well-defined (1×1) -reconstructed surfaces, we consider type 1 spectra showing the largest energy gap as the underlying reference of the Mott gap. Moreover, as we do not observe a clear spatial correlation of any spectral features on disorder, we associate the density of states peaks in the type 2 spectra to defect states in the bulk. Our assumption is that these defect states are directly linked to the defect states responsible for thermally activated transport as well as variable-range-hopping in the system. This approach based on type 2 spectra is able to explain the rather small energy

gaps observed by macroscopic experimental methods, i.e., the bulk transport attributed to thermal conductivity and/or mediated by hopping is provided by the defect states D and D* observed in type 2 spectra.^[8,16,22]

For the explanation of the surface transport, type 2-related conductivity is not well suited, as it freezes out with decreasing temperatures. We therefore propose to attribute the type 3 spectral characteristic to the high 2D surface conductivity, persisting at low temperatures. An important spectroscopic signature is the gap closing via a V-like shape. Deviations from this V-shape are only found at the onset of tunneling into the valence and conduction bulk band states and beyond.

As stated in the discussion of the type 2 spectra, we do not observe a spatial correlation of spectroscopic characteristics on disorder, effectively discarding a disorder-driven insulator–metal transition. Quasiparticle charge transfer induced doping also fails to explain our results, as it only relies on a sufficient amount of sodium adjacent to the respective NaIr_2O_6 layer. Hence, this doping effect must also exist within the bulk, rendering it to not be a distinct surface feature.^[23] In addition, we stated earlier that the sodium content on the Na-terminated surface is even reduced compared with the bulk, further increasing the gap.^[15] This idea is in contrast to the finding, that the $(\sqrt{3} \times \sqrt{3})\text{R}30^\circ$ reconstruction has a smaller bandgap in STS investigations.^[15]

The origin of type 3-related surface conductivity remains rather puzzling. On the one hand, density of states at or close to the Fermi level was found in ARPES.^[16,22,23] On the other hand, our transport measurements reveal extremely high conductivity of the freshly cleaved surface and STS shows an unusual V-like shape close to the Fermi level. Considering that Na_2IrO_3 was predicted to be a 2D or possibly 3D topological insulator, it is tempting to assign type 3 conductivity to be the result of the bulk boundary correspondence for a 3D topological insulator.^[9–11,20,21] Note that the linear dispersion within the Mott gap and the robustness across step edges, as shown in

Figure 3, fit well to this model.^[29,30] The dI/dV curves in Figure 3 are taken across a step edge that separates two terraces with (1×1) -reconstructed surfaces that both exhibit a type 3 spectral characteristic, even though the overall conductivity for small voltages is lower on the bottom terrace. We assign this difference in the apparent conductivity in the STS measurement to extrinsic effects discussed in the Supporting Information. Across the step edge, the spectral characteristic persists, rendering type 3 conductivity to be a 2D feature that is robust across step edges, being in good agreement with the low resistance found in the transport measurements.

Admittedly, the existing ARPES investigations do not see any indication of topological surface states.^[16,22,23] Moreover, we did not observe quasiparticle interference (QPI) pattern at 80 or 300 K.

6. Conclusion

Combining the results from macroscopic temperature-dependent transport with the local spectroscopy information, we propose the following model. Bulk conductivity at higher temperatures is determined by thermally activated carriers from defect-related states and at lower temperatures by hopping between these states, where both processes freeze out with decreasing temperature. In contrast to former experimental studies, we find a clear signature of a low-resistance surface conductivity with a sheet resistance of about $1 \text{ k}\Omega \square^{-1}$, comparable with a $\text{Si}(111)7 \times 7$ surface ($\approx 1.25 \text{ k}\Omega \square^{-1}$ at 300 K) and graphene on 6H-SiC ($\approx 0.6 \text{ k}\Omega \square^{-1}$ at 200 K and $\approx 0.8 \text{ k}\Omega \square^{-1}$ at 300 K).^[31,32] This is an unexpectedly low value considering the high defect density at the Na_2IrO_3 surface and the relatively poor bulk conductance at low temperatures. Our analysis links this high surface conductivity to a V-shaped bandgap closing observed with STS. Combined with the surprising robustness across step edges and against dosing of the surface with air, this supports the idea of a rather unconventional surface conductivity.^[9–11,20–22]

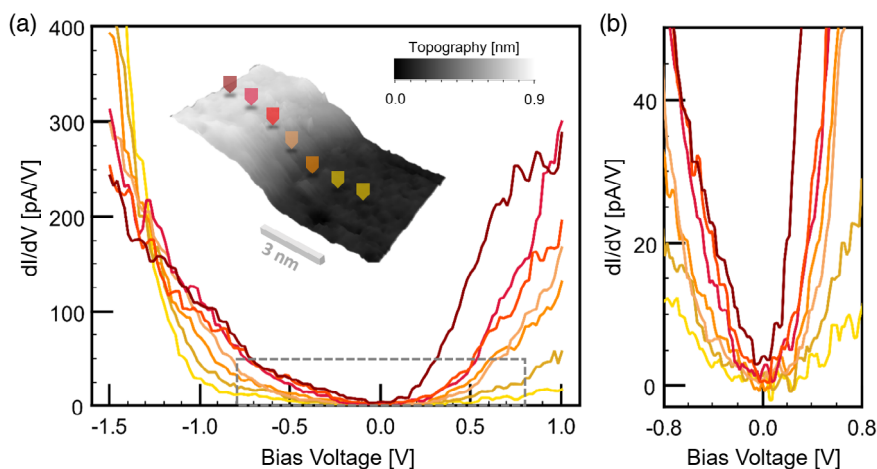


Figure 3. Impact of step edges on type 3 spectra. a) dI/dV spectra recorded equidistantly across a single step on a (1×1) -reconstructed surface. The lateral distance between the spectra is 1 nm. The actual recording positions are marked in the inset and color-coded according to the dI/dV curves. A smooth transition of the curves is observed when crossing the step edge, without any change in the qualitative shape of the spectra. However, the overall conductivity is altered. The deviation regarding the valence band onset at bias voltages lower than -0.8 V is due to the fact that the integral of the dI/dV curves from the setpoint to the Fermi level has to be constant. b) Zoom-in according to the gray dashed box in (a). The bandgap closing resembles a V-shape on an energy scale of several hundred millielectronvolts.

In summary, the nature of the high surface conductance remains an open issue, where the conventional transport mechanisms previously reported for Na_2IrO_3 fail to explain our results. Further investigations will be required to consider rather unconventional electronic properties despite phenomena like nontrivial topology having been discarded up to now.^[22]

Supporting Information

Supporting Information is available from the Wiley Online Library or from the author.

Acknowledgements

The authors thank the Deutsche Forschungsgemeinschaft (DFG) for financial support via Projects 220179758 (SPP 1666) and 107745057 (TRR 80). Data availability: The scanning tunneling microscopy and spectroscopy data sets provided in this work, as well as additional crystal characterization data are available from the authors. Open access funding enabled and organized by Projekt DEAL.

Conflict of Interest

The authors declare no conflict of interest.

Author Contributions

M.W., P.G. and T.D. planned the experiments. T.D., M.W., M. S. and G.T. set up the technical requirements for the experiment. I.P. and P.G. provided the samples and executed their preliminary characterization. T.D. and M.S. carried out the experiments. T.D. and M. W. performed the data analysis. T.D., P.G. and M.W. wrote the manuscript; all authors discussed the results and commented on the manuscript.

Keywords

honeycomb iridate, Mott insulators, Na_2IrO_3 , scanning tunneling spectroscopy, surface conductivity, transport measurements

Received: July 30, 2020

Revised: October 8, 2020

Published online: November 2, 2020

- [1] J. Chaloupka, G. Jackeli, G. Khaliullin, *Phys. Rev. Lett.* **2010**, *105*, 027204.
- [2] Y. Singh, S. Manni, J. Reuther, T. Berlijn, R. Thomale, W. Ku, S. Trebst, P. Gegenwart, *Phys. Rev. Lett.* **2012**, *108*, 127203.
- [3] S. H. Chun, J.-W. Kim, J. Kim, H. Zheng, C. C. Stoumpos, D. Malliakas, J. F. Mitchell, K. Mehlawat, Y. Singh, Y. Choi, T. Gog, A. Al-Zein, M. M. Sala, M. Krisch, J. Chaloupka, G. Jackeli, G. Khaliullin, B. J. Kim, *Nat. Phys.* **2015**, *11*, 462.
- [4] P. Gegenwart, S. Trebst, *Nat. Phys.* **2015**, *11*, 444.
- [5] V. Hermann, J. Ebad-Allah, F. Freund, I. M. Pietsch, A. Jesche, A. A. Tsirlin, J. Deisenhofer, M. Hanfland, P. Gegenwart, C. A. Kuntscher, *Phys. Rev. B* **2017**, *96*, 195137.
- [6] S. M. Winter, Y. Li, H. O. Jeschke, R. Valentí, *Phys. Rev. B* **2016**, *93*, 214431.
- [7] I. I. Mazin, H. O. Jeschke, K. Foyevtsova, R. Valentí, D. I. Khomskii, *Phys. Rev. Lett.* **2012**, *109*, 197201.
- [8] R. Comin, G. Levy, B. Ludbrook, Z.-H. Zhu, C. N. Veenstra, J. A. Rosen, Y. Singh, P. Gegenwart, D. Stricker, J. N. Hancock, D. van der Marel, I. S. Elfimov, A. Damascelli, *Phys. Rev. Lett.* **2012**, *109*, 266406.
- [9] A. Shitade, H. Katsura, J. Kuneš, X.-L. Qi, S.-C. Zhang, N. Nagaosa, *Phys. Rev. Lett.* **2009**, *102*, 256403.
- [10] H.-C. Jiang, Z.-C. Gu, X.-L. Qi, S. Trebst, *Phys. Rev. B* **2011**, *83*, 245104.
- [11] M. Lauenbach, J. Reuther, R. Thomale, S. Rachel, *Phys. Rev. B* **2017**, *96*, 121110.
- [12] D. Pesin, L. Balents, *Nat. Phys.* **2010**, *6*, 376.
- [13] K. Foyevtsova, H. O. Jeschke, I. I. Mazin, D. I. Khomskii, R. Valentí, *Phys. Rev. B* **2013**, *88*, 035107.
- [14] S. Manni, S. Choi, I. I. Mazin, R. Coldea, M. Altmeyer, H. O. Jeschke, R. Valentí, P. Gegenwart, *Phys. Rev. B* **2014**, *89*, 245113.
- [15] F. Lüpke, S. Manni, S. C. Erwin, I. I. Mazin, P. Gegenwart, M. Wenderoth, *Phys. Rev. B* **2015**, *91*, 041405.
- [16] L. Moreschini, I. Lo Vecchio, N. P. Breznay, S. Moser, S. Ulstrup, R. Koch, J. Wirjo, C. Jozwiak, K. S. Kim, E. Rotenberg, A. Bostwick, J. G. Analytis, A. Lanzara, *Phys. Rev. B* **2017**, *96*, 161116.
- [17] F. Ye, S. Chi, H. Cao, B. C. Chakoumakos, J. A. Fernandez-Baca, R. Custelcean, T. F. Qi, O. B. Korneta, G. Cao, *Phys. Rev. B* **2012**, *85*, 180403.
- [18] X. Liu, T. Berlijn, W.-G. Yin, W. Ku, A. Tsvelik, Y.-J. Kim, H. Gretarsson, Y. Singh, P. Gegenwart, J. P. Hill, *Phys. Rev. B* **2011**, *83*, 220403.
- [19] S. K. Choi, R. Coldea, A. N. Kolmogorov, T. Lancaster, I. I. Mazin, S. J. Blundell, P. G. Radelli, Y. Singh, P. Gegenwart, K. R. Choi, S.-W. Cheong, P. J. Baker, C. Stock, J. Taylor, *Phys. Rev. Lett.* **2012**, *108*, 127204.
- [20] C. H. Kim, H. S. Kim, H. Jeong, H. Jin, J. Yu, *Phys. Rev. Lett.* **2012**, *108*, 106401.
- [21] B. H. Kim, K. Seki, T. Shirakawa, S. Yunoki, *Phys. Rev. B* **2019**, *99*, 155135.
- [22] N. Alidoust, C. Liu, S.-Y. Xu, I. Belopolski, T. Qi, M. Zeng, D. S. Sanchez, H. Zheng, G. Bian, M. Neupane, Y.-T. Liu, S. D. Wilson, H. Lin, A. Bansil, G. Cao, M. Z. Hasan, *Phys. Rev. B* **2016**, *93*, 245132.
- [23] J. Rodriguez, G. Lopez, F. Ramirez, N. P. Breznay, R. Kealhofer, V. Nagarajan, D. Latzke, S. Wilson, N. Marrujo, P. Santiago, J. Lara, A. Diego, E. Molina, D. Rosser, H. Tavassol, A. Lanzara, J. G. Analytis, C. Ojeda-Aristizabal, *Phys. Rev. B* **2020**, *101*, 235415.
- [24] Y. Singh, P. Gegenwart, *Phys. Rev. B* **2010**, *82*, 064412.
- [25] A. Vasdev, L. Yadav, S. Kamboj, K. Mehlawat, Y. Singh, G. Sheet, *J. Appl. Phys.* **2018**, *214*, 055102.
- [26] J. W. Krizan, J. H. Roudebush, G. M. Fox, R. J. Cava, *Mater. Res. Bull.* **2014**, *52*, 162.
- [27] Z. Wang, Y. Okada, J. O'Neal, W. Zhou, D. Walkup, C. Dhital, T. Hogan, P. Clancy, Y.-J. Kim, Y. F. Hu, L. H. Santos, S. D. Wilson, N. Trivedi, V. Madhavan, *Proc. Natl. Acad. Sci. USA* **2018**, *115*, 111198.
- [28] I. Battisti, K. M. Bastiaans, V. Fedoseev, A. de la Torre, N. Iliopoulos, A. Tamai, E. C. Hunter, R. S. Perry, J. Zaanen, F. Baumberger, M. P. Allan, *Nat. Phys.* **2017**, *13*, 21.
- [29] M. Z. Hasan, C. L. Kane, *Rev. Mod. Phys.* **2010**, *82*, 3045.
- [30] Y. Ando, *J. Phys. Soc. Jpn* **2013**, *82*, 102001.
- [31] S. Hasegawa, I. Shiraki, T. Tanikawa, C. L. Petersen, T. M. Hansen, P. Boggild, F. Grey, *J. Phys.: Condens. Matter* **2002**, *14*, 8379.
- [32] A. Sinterhauf, G. A. Traeger, D. M. Pakdehi, P. Schädlich, P. Willke, F. Speck, T. Seyller, C. Tegenkamp, K. Pierz, H. W. Schumacher, M. Wenderoth, *Nat. Commun.* **2020**, *11*, 555.